Received: 8 November 2019 | Accepted: 10 March 2020

DOI: 10.1002/sctm.19-0385

TISSUE ENGINEERING AND REGENERATIVE MEDICINE

STEM CELLS TRANSLATIONAL MEDICINE

Tissue-specific mesenchymal stem cell-dependent osteogenesis in highly porous chitosan-based bone analogs

Swati Midha[1] | Krishan G. Jain[1] | Nitu Bhaskar[2] | Amtoj Kaur[1] | Sonali Rawat[1] | Shibashish Giri[3,4] | Bikramjit Basu[2] | Sujata Mohanty[1]

[1]Stem Cell Facility (*Department of Biotechnology-Centre of Excellence for Stem Cell Research*), All India Institute of Medical Sciences, New Delhi, India

[2]Laboratory for Biomaterials, Materials Research Centre, Indian Institute of Science, Bangalore, India

[3]Department of Cell Techniques and Applied Stem Cell Biology, Centre for Biotechnology and Biomedicine, Medical faculty, University of Leipzig, Leipzig, Germany

[4]Department of Plastic Surgery and Hand Surgery, University Hospital Rechts der Isar, Technische Universität München, Munich, Germany

Correspondence
Sujata Mohanty, PhD, Stem Cell Facility (*Department of Biotechnology-Centre of Excellence for Stem Cell Research*), All India Institute of Medical Sciences, New Delhi, India.
Email: drmohantysujata@gmail.com

Shibashish Giri, PhD, Department of Cell Techniques and Applied Stem Cell Biology, Centre for Biotechnology and Biomedicine, Medical faculty, University of Leipzig, Leipzig, Germany.
Email: shibashish.giri@bbz.uni-leipzig.de

Funding information
Department of Biotechnology, Ministry of Science and Technology, Govt. of India; Council of Scientific and Industrial Research, Govt. of India; Department of Science and Technology, Ministry of Science and Technology, Govt. of India

Abstract

Among conventional fabrication techniques, freeze-drying process has widely been investigated for polymeric implants. However, the understanding of the stem cell progenitor-dependent cell functionality modulation and quantitative analysis of early osseointegration of highly porous scaffolds have not been explored. Here, we developed a novel, highly porous, multimaterial composite, chitosan/hydroxyapatite/polycaprolactone (CHT/HA/PCL). The in vitro studies have been performed using mesenchymal stem cells (MSCs) from three tissue sources: human bone marrow-derived MSCs (BM-MSCs), adipose-derived MSCs (AD-MSCs), and Wharton's jelly-derived MSCs (WJ-MSCs). Although cell attachment and metabolic activity [3-4,5-dimethylthiazol-2yl-(2,5 diphenyl-2H-tetrazoliumbromide) assay] were ore enhanced in WJ-MSC-laden CHT/HA/PCL composites, scanning electron microscopy, real-time gene expression (alkaline phosphatase [*ALP*], collagen type I [*Col I*], osteocalcin [*OCN*], and bone morphogenetic protein 4 [*BMP-4*]), and immunostaining (COL I, β-CATENIN, OCN, and SCLEROSTIN [SOST]) demonstrated pronounced osteogenesis with terminal differentiation on BM-MSC-laden CHT/HA/PCL composites only. The enhanced cell functionality on CHT/HA/PCL composites was explained in terms of interplay among the surface properties and the optimal source of MSCs. In addition, osteogenesis in rat tibial model over 6 weeks confirmed a better ratio of bone volume to the total volume for BM-MSC-laden composites over scaffold-only and defect-only groups. The clinically conformant combination of 3D porous architecture with pore sizes varying in the range of 20 to 200 μm together with controlled in vitro degradation and early osseointegration establish the potential of CHT/HA/PCL composite as a potential cancellous bone analog.

KEYWORDS

bone, mesenchymal stem cells, osseointegration, porous, rat model

Krishan G. Jain and Nitu Bhaskar share joint second authorship.

This article was published online on 13 October 2020. An error was subsequently identified in the author affiliation and correspondence sections. This notice is included in both the online and print versions to indicate that they have been corrected on 24 November 2020.

1 | INTRODUCTION

Ultrastructurally, bone is an extracellular matrix (ECM) comprising of hydroxyapatite (HA) [$Ca_{10}(PO_4)_6(OH)_2$] as mineral phase and type I collagen, as the organic phase.[1] Taking cues from the bone nanostructure, composite materials, such as polymer/ceramic composites, have emerged as potential scaffolds possessing appropriate mechanical properties and cytocompatibility.[2,3] Polycaprolactone (PCL) is a biocompatible polymer with slow degradation rate and is blended with other polymers, such as chitosan (CHT),[4] polylactic acid,[5] and gelatin[6] to improve stress crack resistance, flexibility, wettability, and biodegradation. CHT is preferred owing to its biodegradable, biocompatible, nontoxic nature and reactive functional groups.[7] Addition of CHT results in enhanced wettability, accelerated degradation of PCL, and improved cytocompatibility in composites.[4] Despite promising data, studies investigating PCL/CHT composites are still in their nascent state.

Potential scaffolds designed for bone applications must take into consideration the load-bearing function of bone to withstand large forces (equivalent to or greater than body weight)[8] and to promote osseointegration at early stages of implantation to prevent implant loosening and rejection. Ceramic particles like HA are added to composites in order to promote early bone integration.[9] HA nanoparticles act as centers of calcification; akin to natural bone structure, reinforce the material strength and promote direct and rapid bonding to the surrounding host bone matrix. Physical parameters, like scaffold porosity, pore size, and 3D geometry also play an integral role in deciding the efficacy of the scaffolds to be used for bone regeneration. Pore sizes, ranging from micro- to macropore, appropriately mimic the stochastic model of natural bone. Well-interconnected pores support better cell penetration, neotissue ingrowth, faster nutrient diffusion, neovascularization, and waste removal,[4] thereby making porous polymer/ceramic composites ideal for bone substitution.

Besides the material, choice of correct cell type is imperative to the process of bone formation, especially in the case of critical-sized defects. To restore large clinical defects, surgeons often harvest a part of the patient's marrow from the iliac crest and add them to bone graft substitutes prior to implantation. Among all the available sources, bone marrow-derived mesenchymal stem cells (BM-MSCs) and adipose-derived MSCs (AD-MSCs) are popular cell choices for bone regenerative applications.[10,11] Although BM-MSCs have proven clinical advantages, AD-MSCs possess some attractive characteristics, such as abundant stem cell source from lipoaspirates, faster proliferation rate and lesser discomfort, and morbidity to the patient.[12] However, their osteogenic potential is still somewhat debated. Wharton's jelly-derived MSCs (WJ-MSCs) are a relatively new source of MSCs. They have garnered interest owing to their high cell yield and easy isolation from amniotic membranes, which are a biological waste, hence making the collection process pain-free and easy.[13] But comprehensive understanding of the stem cell progenitor-dependent cell functionality modulation has not been well investigated. To this end, one of the primary aims of this study was to compare the extent of osteogenic differentiation in vitro between the three tissue-specific human MSCs (hMSCs) as a function of their origin.[14,15] The study was intended to provide answers to some clinically relevant questions around appropriate combinations of synthetic bone substitutes and cells for translational therapy.

Significance statement

A porous, multimaterial composite was developed using an easy and economical method, which mirrors the stochastic geometry of bone. Three tissue-specific human stem cells of clinical relevance (bone marrow-, adipose-, and fetal-derived mesenchymal stem cells [MSCs]) evaluated for early osseointegration revealed superior bone formation in bone marrow MSC-laden composites in rat tibial defects.

Herein, we have developed porous 3D CHT/HA/PCL composite to test its potential in bone regeneration. We have attempted to address the following unanswered questions: Whether CHT/HA/PCL composites are suitable candidates for bone formation? This includes learning about early osseointegration potential of CHT/HA/PCL and their potential to withstand load-bearing in situ. Which source of MSCs (BM vs AD vs WJ) is most suitable for bone differentiation on these composites? Whether cell-laden CHT/HA/PCL composites can facilitate terminal differentiation of stem cell progenitors towards mature bone phenotype? The in vitro cytocompatibility assessment was conducted using cytotoxicity analysis, cell attachment, gene expression profiling, and immunostaining. Subsequently, in vivo biocompatibility in rat orthotopic load-bearing defects was evaluated at a relatively early time point, that is, week 6 using microcomputed tomography (micro-CT) analysis and histology. The present study generated significant insights into the choice of cell type and the physical parameters of the 3D porous composite that guides cellular differentiation of hMSCs towards mature, osteogenic lineage on CHT/HA/PCL matrices, both in vitro and in vivo.

2 | MATERIALS AND METHODS

2.1 | Materials

The chitosan, CHT (weight average molecular weight, M_w 70 000-90 000 Da, density 1.145 g mL^{-1} at 25°C, degree of deacetylation 90%), HA (M_w 502.31 Da and particle size <200 nm), PCL (M_w 48 000-90 000 Da, melt index 1.8 g per 10 minutes, 80°C), 3-4,5-dimethylthiazol-2yl-(2,5 diphenyl-2H-tetrazoliumbromide) (MTT), dimethylsulfoxide, lysozyme, and osteogenic supplements (dexamethasone, ascorbic acid-2 phosphate, and β-glycerophosphate) were procured from Sigma-Aldrich (St. Louis, Missouri). Cell culture reagents

including low-glucose Dulbecco's modified Eagle medium (DMEM-LG), fetal bovine serum (FBS), L-glutamine, penicillin/streptomycin and trypsin-ethylenediaminetetraacetic acid (EDTA) were procured from Gibco, Thermoscientific. Sodium hydroxide (NaOH), glacial acetic acid, and other reagents were of analytical grade.

2.2 | Methods

2.2.1 | Scaffold fabrication and synthesis

The scaffolds were fabricated as previously described.[16] Briefly, CHT/HA/PCL in the ratio of 3:3:2 (wt/vol) was lyophilized (Coolsafe 110-4, labogene, Lynge, Denmark). HA powder (3% wt/vol) was dispersed in acetic acid (2 mM) to which CHT (3% wt/vol) was dissolved. PCL (2% wt/vol) was added to CHT/HA solution, immediately casted into plastic molds, and freeze-dried at −80°C for 48 hours. Freeze-dried composite foams were soaked in NaOH (2 M) for 2 hours to neutralize the acid. The scaffolds were punched into disks for further studies.

2.2.2 | Physicochemical characterization of composites

SEM and energy-dispersive X-ray analysis

The morphology of CHT/HA/PCL was examined by Zeiss EVO18 scanning electron microscope (Cambridge Scientific Industries, Watertown, Massachusetts). The average pore diameter was measured using the NIH Image J software (Dr Wayne Rasband, National Institutes of Health, Bethesda, Maryland) across 300 pores in five randomly selected images. For cell-laden CHT/HA/PCL composites (n = 3), specimens were fixed, dehydrated, sputter coated, and imaged. For energy-dispersive X-ray (EDX) analysis, samples were carbon-coated and imaged.

Porosity

The porosity of CHT/HA/PCL was measured using liquid displacement method[17] as follows:

$$\text{Degree of porosity}\,(\%) = 100 \times (W_1 - W_0)/\rho V_0,$$

where W_0 and V_0 are the initial weight and volume of composite, respectively; W_1 is the final weight of composite post-immersion; and ρ represents the density of *n*-hexane.

In vitro degradation

Composites (n = 3) of 9 mm × 9 mm × 2 mm dimensions were weighed (W_0) and placed in glass vials with lysozyme solution (100 mg L^{-1} lysozyme diluted in phosphate-buffered saline, PBS) in a shaker at 37°C with solution changed twice a week. The samples were removed at 1, 2, 3, 4, 5, and 6 weeks, respectively, rinsed, freeze-dried for 36 hours, and weighed (W_t). The in vitro degradation of composites was monitored as the % loss in weight over time :

$$\%\text{Weight loss} = (W_0 - W_t)/W_0 \times 100.$$

Static contact angle

A drop of deionized water (1 μL) was placed on the composite to determine the water contact angle using a goniometer (LINOS, FLS 95-750 M, Germany).

Hydration efficiency

CHT/HA/PCL composites (n = 3) were immersed in 1× PBS, pH 7.4 at 37°C for 24 hours and their respective weights pre-immersion (W_0) and post-immersion (W_w) were recorded. The hydration efficiency was determined as follows:

$$\text{Hydration efficiency} = (W_w - W_0)/W_0 \times 100.$$

Permeability

Qualitative estimation of permeability was performed on CHT/HA/PCL (diameter = 1 cm, height = 4 and 8 mm) using trypan blue as a measure of dye penetration. After allowing sufficient time (~2 minutes) for dye penetration, composites were cross-sectioned and imaged.

X-ray diffraction

For X-ray diffraction (XRD) analysis, composites were scanned within 10° to 80° (2θ) range at a speed of 2° min^{-1} using a Siemens type F X-ray diffractometer with Cu K_α radiation.

Fourier transform infrared spectroscopy

Fourier transform infrared spectroscopy (FTIR) was carried out within 400 to 4000 cm^{-1} at 4 cm^{-1} resolution with a total of 50 scans taken using deuterated triglycine sulfate with IR detector (Spectrum BX Series, Waltham, Massachusetts) .

2.2.3 | In vitro cytocompatibility analysis

Cell culture and seeding on composites

Cryopreserved human BM-MSCs, AD-MSCs, and WJ-MSCs were revived, expanded and characterized as before.[18] The study was performed in accordance with the Institutional Review Committee guidelines at AIIMS, New Delhi, and informed patient consents were obtained [IC-SCR/79/18(o)]. Cells were expanded in DMEM-LG supplemented with 10% FBS, L-glutamine (2 mM), and 1% penicillin/streptomycin at 37°C in 5% CO_2 and 95% humidity. For cell culture, sterilized composites were seeded with 5×10^4 cells/composite and cultured for 21 days in osteogenic differentiation media.[19]

Cell attachment, live/dead staining, and cytotoxicity assessment

After 12 hours, cell-laden composites were trypsinized, trypan blue stained, and counted to compute cell attachment.[20] 2D monolayer culture served as controls. The data were expressed in terms of % live cells. Live/dead staining (K501-100, Biovision, Milpitas, California) of

BM-MSC-laden composites was performed at day 7 and imaged using confocal laser scanning microscope (TCS SP5, Leica, Germany). Cytotoxicity assessment of cell-laden composites for the three cell types was performed using MTT assay up to 21 days,[20] and readings were obtained using plate reader (EL 800, Biotek, Winooski, Vermont).

Quantification of bone-specific gene expression

After 21 days, quantitative real-time polymerase chain reaction (qRT-PCR, Biorad-CFX96) was performed on cell-laden composites (n = 3) containing the three hMSC types via $2 - (\Delta\Delta c[t])$ method. RNA was isolated using trizol method and purity and concentration was assessed (Nanodrop, Implen, Germany). First-strand cDNA synthesis was performed as per manufacturer's instructions (Thermo Scientific, Cat No. 4368814). SYBR Green Master Mix (KAPA Biosystems, Cat No. KK4601) was used. Osteogenic primers used were collagen type I (*Col I*), alkaline phosphatase (*ALP*), osteocalcin (*OCN*), and bone morphogenetic protein 4 (*BMP-4*) [sequences in Table S1]. Glyceraldehyde-3-phosphate-dehydrogenase (*GAPDH*) was the housekeeping gene. Data were normalized to their respective uninduced (without osteogenic medium) cell-laden composite cultures. Uninduced groups refer to BM-MSC, AD-MSC, and WJ-MSC cultured on composites under nonosteogenic conditions. For plotting the graph, we have taken uninduced group as 1 and plotted others as relative groups (BM-MSC, AD-MSC, WJ-MSC) cultured in osteogenic conditions on composites.

Immunofluorescence analysis

BM-MSC, AD-MSC, and WJ-MSC-laden composites were harvested and stained for (a) anti-COL I (Invitrogen), (b) anti-β-CATENIN (Millipore), (c) anti-osteocalcin (OCN, Invitrogen), and (d) anti-SCLEROSTIN (SOST, Invitrogen), followed by secondary antibody: Alexa Fluor 546 goat anti-mouse IgG antibody-FITC (Fluorescein isothiocyanate) conjugate (Millipore) and Alexa Fluor 488 goat anti-mouse IgG antibody (Millipore). Stage-specific staining was performed using COL I at day 7, β-CATENIN and OCN at day 14, and SOST at day 21.[1] Phalloidin staining was used to visualize the cytoskeletal arrangement of seeded cells and 4′,6-diamidino-2-phenylindole (DAPI) for nuclei (Sigma-Aldrich). Imaging was done using Leica TCS SP5 (Leica Microsystems) microscope.

2.2.4 | In vivo osseointegration

All animal surgeries were performed with prior approval from the Institutional Animal Ethics Committee at AIIMS, New Delhi (41/IAEC-1/2017). Briefly, 15 Wistar rats (male, 10-12 weeks old, 230-270 g) were anesthetized (ketamine:xylazine) and a 3-mm load-bearing defect was created using a trephine bur.[21] Rats were categorized into three groups (n = 5); CHT/HA/PCL dry, CHT/HA/PCL with undifferentiated BM-MSCs cultured for 7 days in vitro, and defect only. Rats were housed in clean cages with access to food and water ad libitum. After 6 weeks, rats were euthanized and their tibiae were harvested for micro-CT, histology, and immunofluorescence staining.

Micro-CT analysis

The micro-CT analysis for neobone formation around the composites with respect to rat tibial bone (sham control) were accomplished using X-ray micro-computed tomography (VersaXRM-500, Xradia, Zeiss, Germany) of high resolution. The scanning was carried out at X-ray beam energy = 70 kV, power = 7 W, and current = 87 μA. A 4 × objective with exposure time of 3 s was availed for image acquisition which was totally dependent on samples. The alternance in the density of host bone and the implant was the basis of extracting the 3D image of the implant. Also, the obtained 3D images were acquired on the basis distinction between VOI (volume of interest) and ROI (region of interest). The complete timing of scan was 3 000 000 ms with the collection of 2001 projection images. The standard beam hardening correction and Gaussian smoothening was used for reforming the 3D tomogram from the transmission images with the help of XM Reconstructor (Xradia, Zeiss, Germany). In order to assess the percentage bone ingrowth inside the defect, the Avizo image-processing software was used to get 3D images of the composite bone implant. A cylindrical ROI in tibia bounded by the biomaterial phase was chosen for analysis from obtained CT scan database. This ROI was further optimized for segmentation to get various sectioned images in all the dimensions. The thresholds were appropriately applied to volume rendered images of each sample in order to visualize and distinguish the neo bone formation from the residual scaffold. The percentage of bone ingrowth was measured as, bone volume (BV) to the total volume (TV) ratio, also known as bone volume fraction (BV/TV). This was determined for different samples after thresholding and segmentation. Bone volume (BV) and total volume (TV) was obtained by counting the total number of bone voxels and total number of voxels (bone and nonbone), respectively in images.

Histology

Formalin-fixed tibiae were decalcified, embedded in paraffin for attaining 5 μm thick sections[21] and stained for hematoxylin and eosin (H&E) and Masson's trichrome.

2.3 | Statistical analysis

GraphPad Prism 5 was used for plotting data with results presented as mean ± SD (for in vitro studies, n). Two-way analysis of variance and Bonferroni post hoc tests were performed to compute statistical significance, where probability (*P*) *value of* ≤ .05 was considered as statistically significant.

3 | RESULTS

3.1 | Physicochemical characterization of hybrid composites

The freeze-drying based processing approach allowed us to obtain CHT/HA/PCL composites with large pore size distribution (Figure 1).

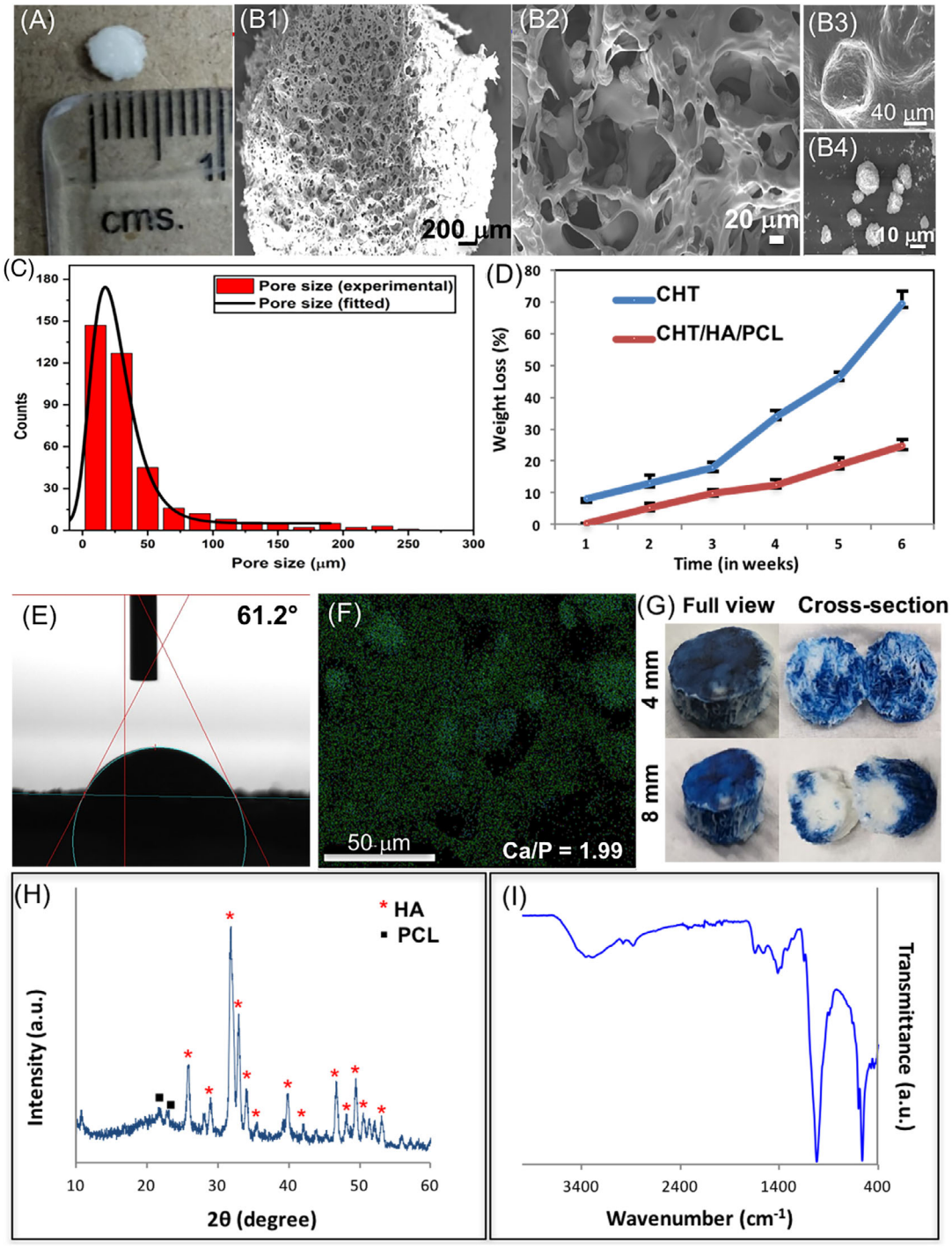

FIGURE 1 Physical characterization of CHT/HA/PCL. A, Digital image; B1-B4, SEM micrographs, B1,B2, depict morphology and pore geometry of composite; B3, PCL; B4, HA; C, pore size distribution; D, degradation kinetics of CHT/HA/PCL in lysozyme; E, static contact angle; F, EDX analysis showing the elemental distribution over the selected microstructural region (Ca-rich area); G, permeability assessed by trypan blue penetration; H,I, physicochemical characterization of CHT/HA/PCL using, H, XRD patterns and, I, FTIR spectra. Data represents mean ± SD of five independent experiments. CHT, chitosan; EDX, energy-dispersive X-ray; FTIR, Fourier transform infrared spectroscopy; HA, hydroxyapatite; PCL, polycaprolactone; SEM, scanning electron microscopy; XRD, X-ray diffraction

Microparticles observed on the composite surface were PCL (Figure 1B3), with a relatively smoother appearance and HA (up to several microns in diameter),[22] with coarse texture (Figure 1B4). Ca/P ratio of HA as determined by EDX was 1.99 (Figure 1F). A slight deviation was obtained from the typical Ca/P ratio of HA, that is, 1.67[4] which might be the effect of processing parameters used in the fabrication of CHT/HA/PCL composite. The agglomeration of HA limits the use of higher amount, which tend to settle unless constantly stirred.[23] The

in vitro degradation after 6 weeks in lysozyme (Figure 1D) showed that degradation of CHT only was greater than CHT/HA/PCL. The blending of HA and PCL with CHT significantly decreased the weight loss, in vitro. Hydrophilicity of CHT leads to an increased water absorption, resulting in hydrolytic degradation.[4] Hydration efficiency of the composite was high corresponding to 205.28% ± 6.43% (Table S2). The water contact angle on CHT/HA/PCL was 61.2° (Figure 1E), which is significantly lesser than that of pure PCL (110°-150°). This indicates that the mixing of CHT and HA to PCL makes the scaffold hydrophilic.[24,25] The increased hydrophilicity may be attributed to the presence of reactive functional groups of CHT[7] and HA.[24,26] Increased hydrophilicity facilitates more transport efficiency of the construct for higher cell attachment and tissue regeneration; however, excessive hydration may affect structural integrity. Permeability test (Figure 1G) showed that trypan blue dye conspicuously covered the cross-sectional region of composites indicating efficient fluid infiltration, but only in samples measuring up to 4 mm in height. XRD of CHT/HA/PCL exhibited characteristic peaks at 31.8° and 25.8° indicating (211) and (002) planes of HA, as depicted in Figure 1H.[22,27] CHT, being a polymer, produced a diffraction halo between 15° and 25°.[28] For PCL, the primary peak at (110) plane corresponded to 2θ = 21.6° and the weaker peak (200) was found at 2θ = 23°, attributing to its semicrystalline character.[29] A small shoulder peak is present at 2θ = 23° suggesting the blending of PCL/CHT.[29]

Attenuated total reflection-FTIR (ATR-FTIR) absorbance spectra were studied to determine the molecular interactions among CHT, HA, and PCL (Figure 1I). HA showed characteristic peaks[22] at 471, 565, and 602 cm^{-1} corresponding to O-P-O bending and at 1029 cm^{-1} for P-OH stretching. The presence of hydroxyl (OH^-) ions, indicated by the presence of IR band at 632 cm^{-1} was missing. This is common with poorly crystallized apatites.[26] The bands at 3360,[30] 2929, 1630, 1367, and 1157 cm^{-1} were attributed to CHT.[28,31] Slight shift in the peak for N—H bending (1565 to 1602 cm^{-1}; red shift) was attributed to electrostatic interactions between CHT and HA.[32,33] The band at 2999 cm^{-1} (C—H stretching) and 1306 cm^{-1} indicated crystalline phase of PCL.[30] The peak at 1727 cm^{-1} (carbonyl stretching) was not present which may be due to masking by CHT. Overall, PCL and CHT retained their native polymer properties.[34]

3.2 | In vitro cytocompatibility

3.2.1 | Cell attachment

Cell attachment for the three tissue-specific hMSC-laden composites on day 1 were in the order of WJ-MSCs (85.7%) > BM-MSCs (79%) > AD-MSCs (74%). 2D cell culture was taken as positive control.

3.2.2 | Cell viability

BM-MSC-laden composites monitored using live/dead assay (Figure 2) revealed that 87.5% of the total cell population stained live (green fluorescence) after 7 days. MTT assay performed over 21 days showed an increasing trend of cell activity in all three cell-laden composites in the order of AD-MSCs < BM-MSCs < WJ-MSCs. The maximal cell metabolic activity of WJ-MSCs by day 21 ($P \leq .01$) may be attributed to their neonatal source of origin.[35,36]

3.2.3 | Cellular morphology

Interestingly, SEM micrographs revealed drastic variation in the morphology of the three tissue-specific hMSCs, cultured on the composites for 21 days (Figure 3A). In BM-MSC-laden composites, typical fibroblastic cellular morphology within the range of 20-100 μm[37] was evident by day 7. By day 14, cells appeared to shrink in size (20-30 μm) displaying numerous protrusions (yellow arrowhead) acquiring a stellate-shaped morphology. These are characteristic of terminal osteocytic differentiation, which represents the primary (90%-95%) resident cell population of cortical bone.[38] EDX demonstrated Ca/P ratio of 1.31 (Figure 3B). By day 21, several osteocyte-like cells were evident, establishing close networks within the ECM.

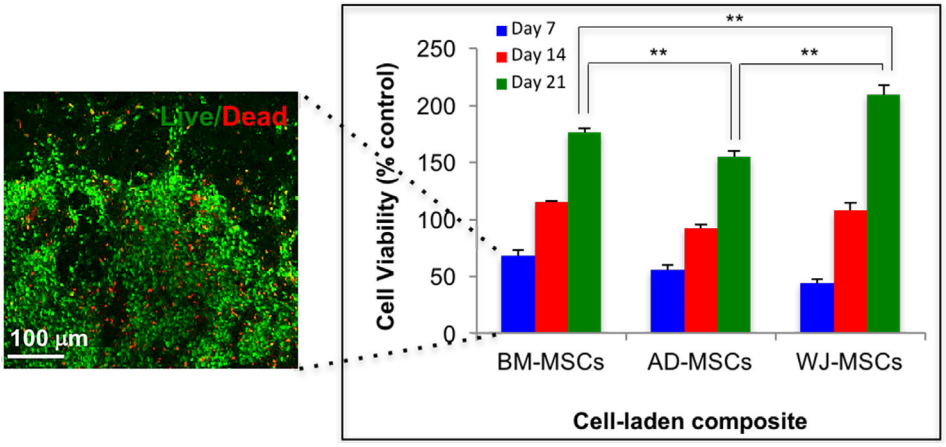

FIGURE 2 Cell metabolic activity of the three MSC-laden composites assessed using MTT assay up to 21 days in vitro. Significance of probability is represented as follows: $^{**}P \leq .01$. The adjacent image shows a representative confocal micrograph of live/dead (green/red) staining performed on BM-MSC-laden composite at day 7. BM-MSC, bone marrow-derived MSCs; MSC, mesenchymal stem cell; MTT, 3-4,5-dimethylthiazol-2yl-(2,5 diphenyl-2H-tetrazoliumbromide)

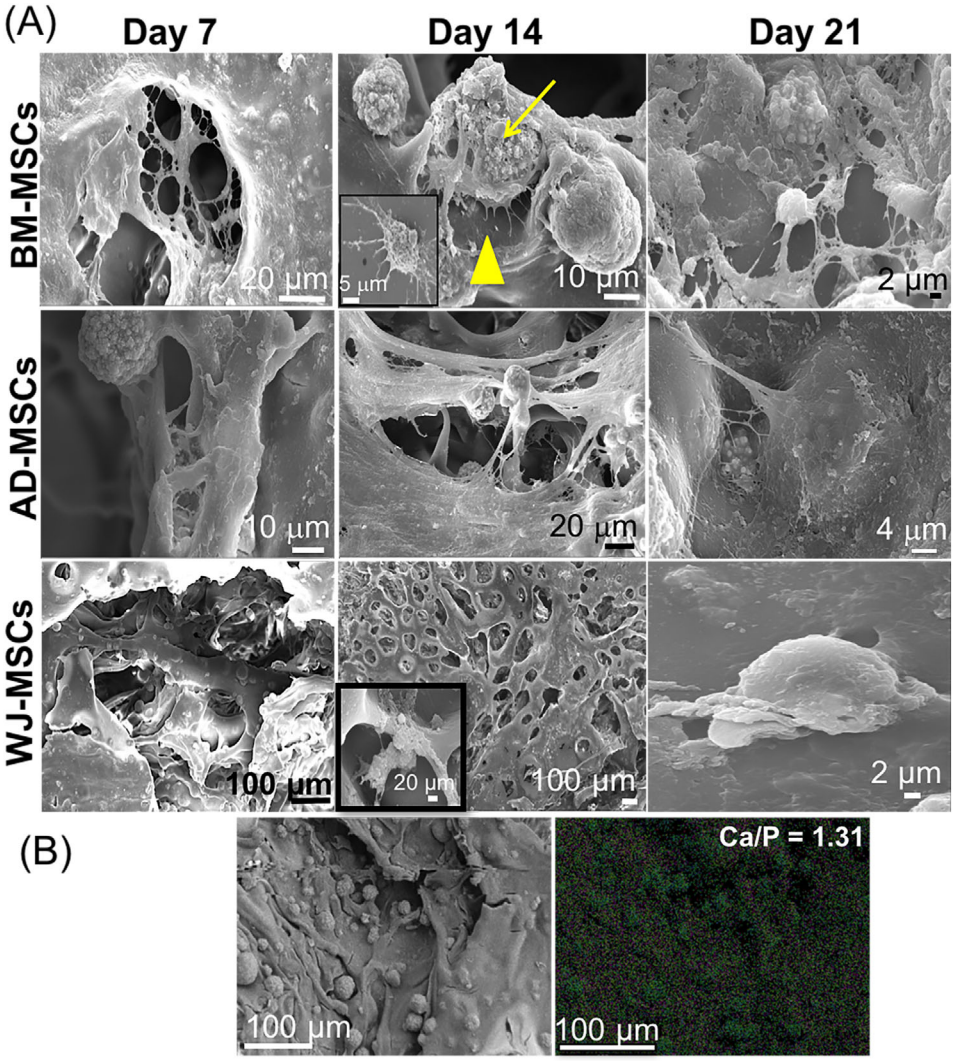

FIGURE 3 A, SEM micrographs of the three tissue-specific hMSCs cultured over CHT/HA/PCL over the 21-day culture period. The yellow arrowhead in BM-MSC-laden composite at day 14 points toward the cellular protrusions arising from the transition of osteoblast to osteocyte phenotype. B. EDX analysis showing the elemental map to determine the overall composition of the biomineralized surface on the BM-MSC-laden composites. The area selected for EDX analysis is represented by the adjacent (left) SEM micrograph. CHT, chitosan; BM-MSC, bone marrow-derived MSCs; EDX, energy-dispersive X-ray; HA, hydroxyapatite; hMSCs, human MSCs; MSCs, mesenchymal stem cells; PCL, polycaprolactone; SEM, scanning electron microscopy

AD-MSCs attained a similar fibroblastic morphology by day 7 with subsequent encapsulation of cells within a dense ECM. No noticeable evidence of mineralization was observed on AD-MSC-laden composites.

WJ-MSCs demonstrated dense matrix formation on the composite surface that resembled more of a confluent cell sheath rather than a cell-synthesized matrix due to faster proliferation of WJ-MSCs (Figure 3A). WJ-MSC-laden composites typically demonstrated cell clusters, with few areas where single cells were identified (inset) with minimal attachment to the composite surface, suggesting weak cell-matrix interactions.

On the other hand, all three hMSCs were cultured on tissue culture plastic to validate the differentiation status of cells, in parallel experiments. BM-MSCs and AD-MSCs showed distinct signs of matrix synthesis and cellular differentiation up to day 21, with little osteogenic differentiation in WJ-MSCs (Figure S1). Overall, superior osteogenic phenotype of BM-MSCs over other cells was marked by (a) mature and phenotypically stable cells, (b) strong cell-matrix interactions, and (c) matrix synthesis and mineralization.

3.2.4 | Gene expression analysis

ALP is a distinct marker for bone mineralization in situ.[39] Comparative analysis shows the highest *ALP* expression for AD-MSC and lowest for WJ-MSC-laden composites, as reported earlier.[13] Significantly higher *ALP* in AD-MSCs over BM-MSCs was observed. Previous studies have reported that with increased osteocytic phenotype, *ALP* expression level decreases,[40] which explains the decreased *ALP* activity in BM-MSC-laden composites over AD-MSC-laden composites by day 21.

Col I is an early stage osteogenic marker responsible for extracellular matrix formation (ECM).[1] Trend shows that expression of *Col I* was highest in BM-MSC-laden composites after 21 days showing approximately two times increase over AD-MSCs (Figure 4A); this is in accordance with previous in vitro[41] and in vivo[42] findings. A negligible level

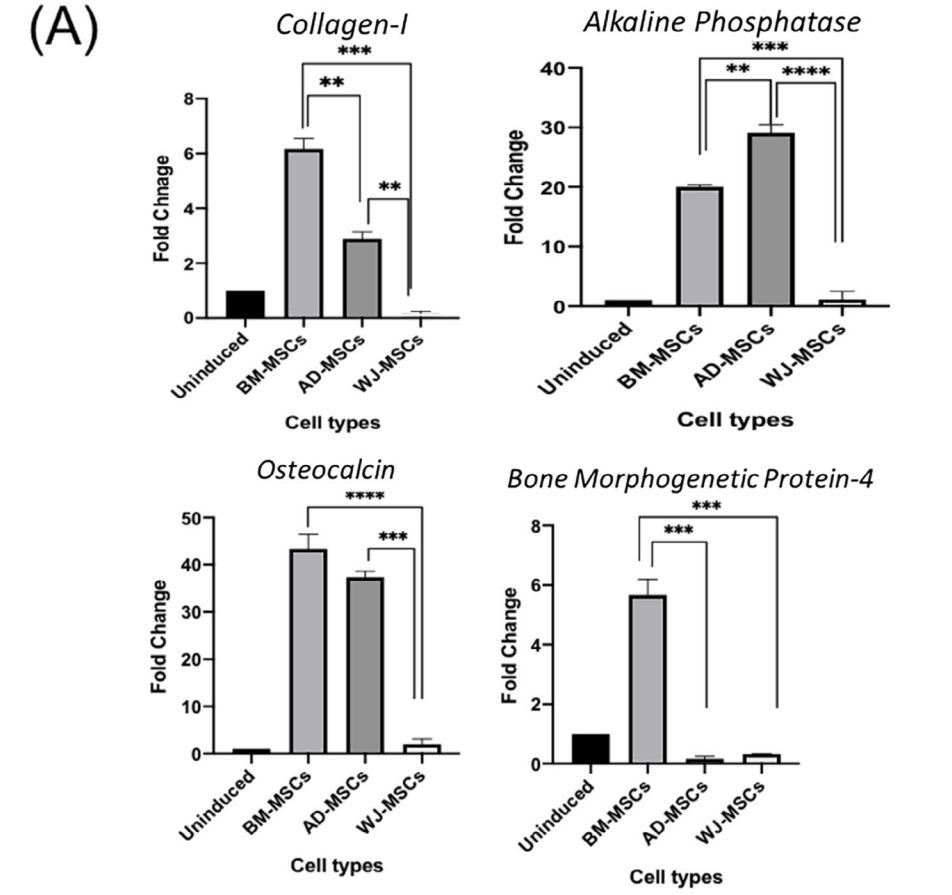

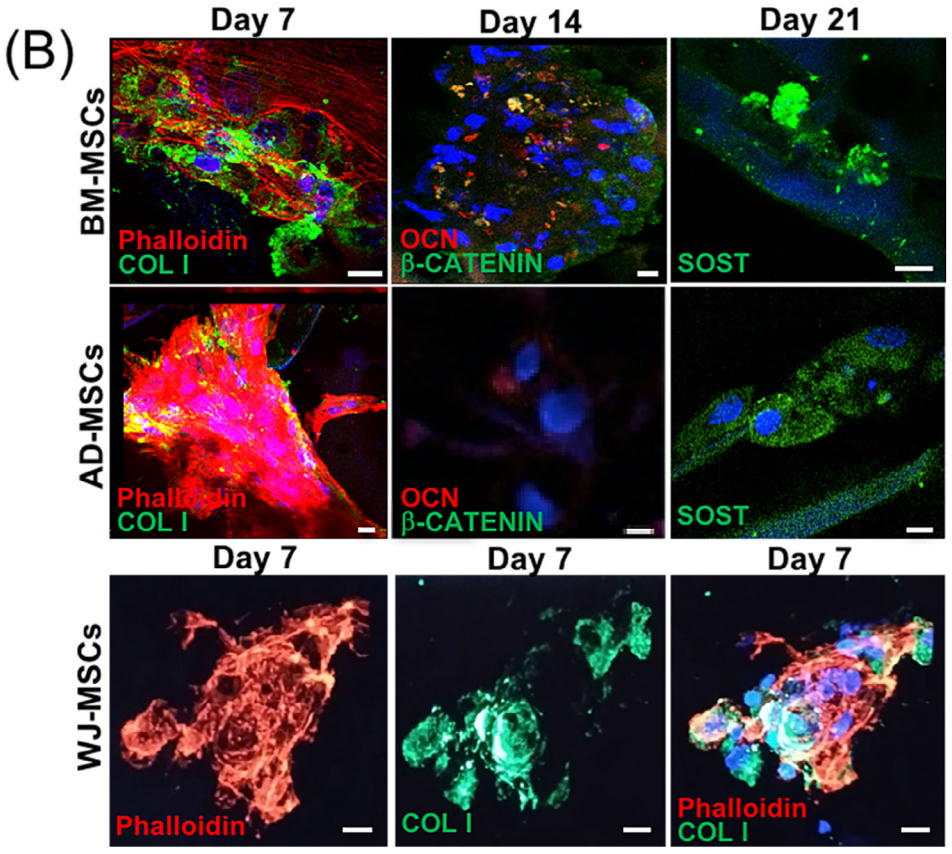

FIGURE 4 A, Real-time gene expression profiles of osteogenic markers expressed in the three tissue-specific hMSCs cultured on CHT/HA/PCL composites for 21 days. Significance of probability is represented as follows: $^{*}P \leq .05$; $^{**}P \leq .01$; $^{***}P \leq .001$. Values are expressed as mean ± SD, with n = 3 per group. B, Confocal micrographs of the tissue-specific hMSCs cultured on CHT/HA/PCL composites stained for COL I (green) at day 7, OCN (red), β-CATENIN (green) at day 14, and SOST (green) at day 21 of osteogenic differentiation. DAPI (blue) was used for nuclear staining. Scalebars = 10 μm. COL I, collagen type I; CHT, chitosan; DAPI, 4′,6-diamidino-2-phenylindole; HA, hydroxyapatite; hMSCs, human MSCs; MSCs, mesenchymal stem cells; *OCN*, osteocalcin; PCL, polycaprolactone; SOST, sclerostin

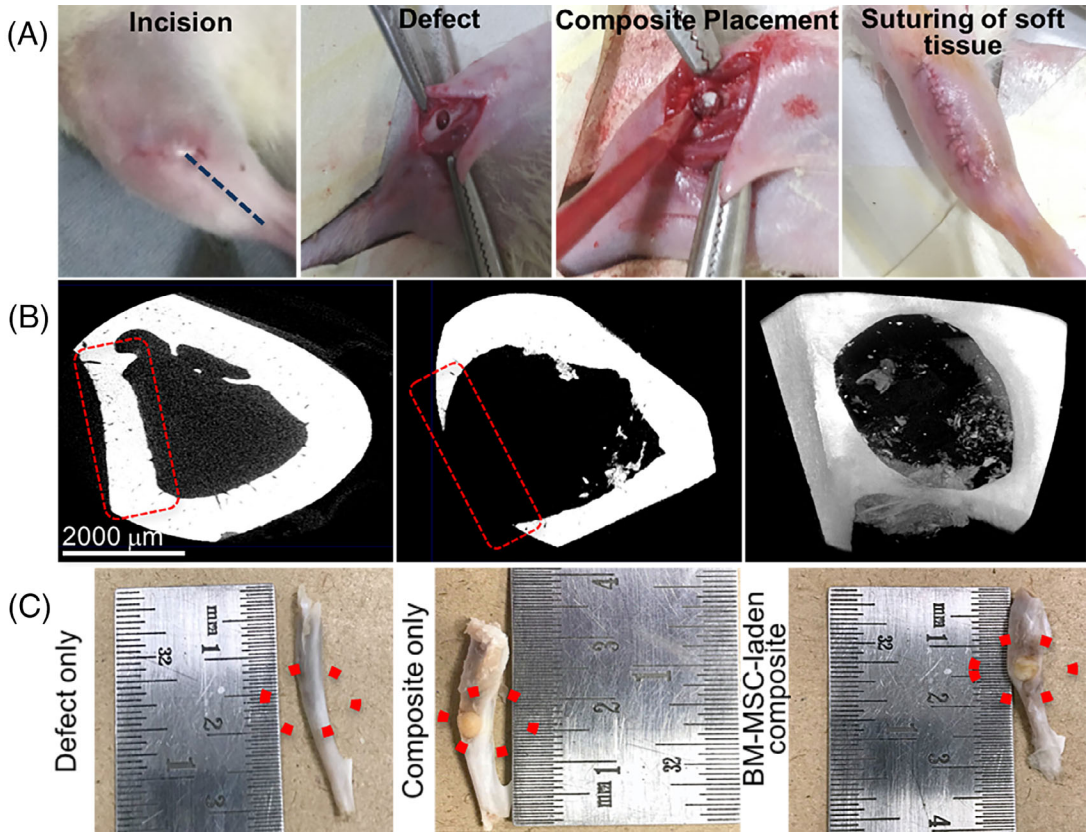

FIGURE 5 A, Surgical scheme for developing rat tibial defect model. B, Micro-CT images depict the region of interest (red dotted lines) with the defect created at day 0 in trans-axial slice and frontal frame, respectively. Gross examination of ex vivo samples of rat tibiae harvested 6 weeks post surgery. The composite appears to be well integrated inside the bone defect. Control or defect-only tibiae show a slight dent on the external surface. Red dotted circles indicate the region of interest. Micro-CT, microcomputed tomography

of expression was noticed in WJ-MSC-laden composites in terms of fold change. Being an early marker, *Col I* usually peaks during the first week of culture (as evident from the discrete florescence staining in Figure 4B), and the expression levels decline thereafter[20,43]; therefore, the relatively lower gene expression pattern of *Col I* in our study was due to the late time point (day 21) of analysis.

OCN, indicative of bone mineralization, showed statistically significant increase in BM-MSC-laden composites over AD-MSCs after 21 days. This was further confirmed by immunostaining (Figure 4B). *BMP-4*, an osteogenic signaling molecule, having critical role in bone development,[44] was majorly expressed in BM-MSC-laden composites. WJ-MSCs showed minimal osteogenic expression for all markers tested. Our results are largely in accordance with the literature in terms of the extent of osteogenesis reported in the order of BM-MSCs > AD-MSCs > WJ-MSCs (Figure 4B).[14,45,46]

3.2.5 | Immunofluorescence analysis

Markers spanning the different stages of osteogenesis, including early (COL I), mid (β-CATENIN), late (OCN, and osteocytic (SOST) differentiation, were analyzed for protein synthesis in cell-laden composites using immunofluorescence staining (Figure 4B). Phalloidin staining demonstrated extensively elongated stress fibers of BM-MSCs (Figure 4B), suggesting enhanced cell-material interactions. By day 7, COL I staining revealed that matrix synthesized by BM-MSCs was typically collagen type I; the most abundant ECM protein in bone.[1] β-CATENIN staining (green) in BM-MSC-laden composites indicated involvement of Wnt/β-catenin signaling in directing cellular differentiation. Discrete patches of OCN (red) provided strong evidence of mineralization. SOST staining, suggesting mature osteocytic cell phenotype, was only evident in BM-MSC-laden composites. The background staining observed in some images was due to the material interference.

In the case of AD-MSCs, all osteogenic markers were less discrete as compared to BM-MSCs (Figure S2). Although AD-MSC-laden composites synthesized abundant COL I the intensity of β-CATENIN and OCN was noticeably reduced. In WJ-MSCs, most of the COL I was visible mainly due to clumping of the cells (cell-cell interaction), indicating lesser affinity of cells toward the scaffold surface (cell-matrix interaction). Negligible staining for OCN, β-CATENIN, and SOST were observed in WJ-MSC-laden composites (data not shown).

2D fluorescence micrographs of the respective hMSCs when cultured on tissue culture plastic demonstrated a similar order of cellular

differentiation, with BM-MSCs > AD-MSCs > WJ-MSCs, as shown by COL I staining (Figure S2).

3.3 | In vivo evidence of bone formation

Based on the in vitro screening data, we selected BM-MSC-laden CHT/HA/PCL composites for the in vivo study. The detailed surgical scheme is depicted in Figure 5A. Ex vivo scans at day 0 displayed a uniform, circular defect, spanning the medial wall of tibia (Figure 5B). After 6 weeks of implantation in rats, gross examination of ex vivo samples showed complete integration of the composites inside the defect site (Figure 5C). In the control defects, a slight dent in the bone was observed in the defect site due to partial healing of the tibia in 6 weeks.

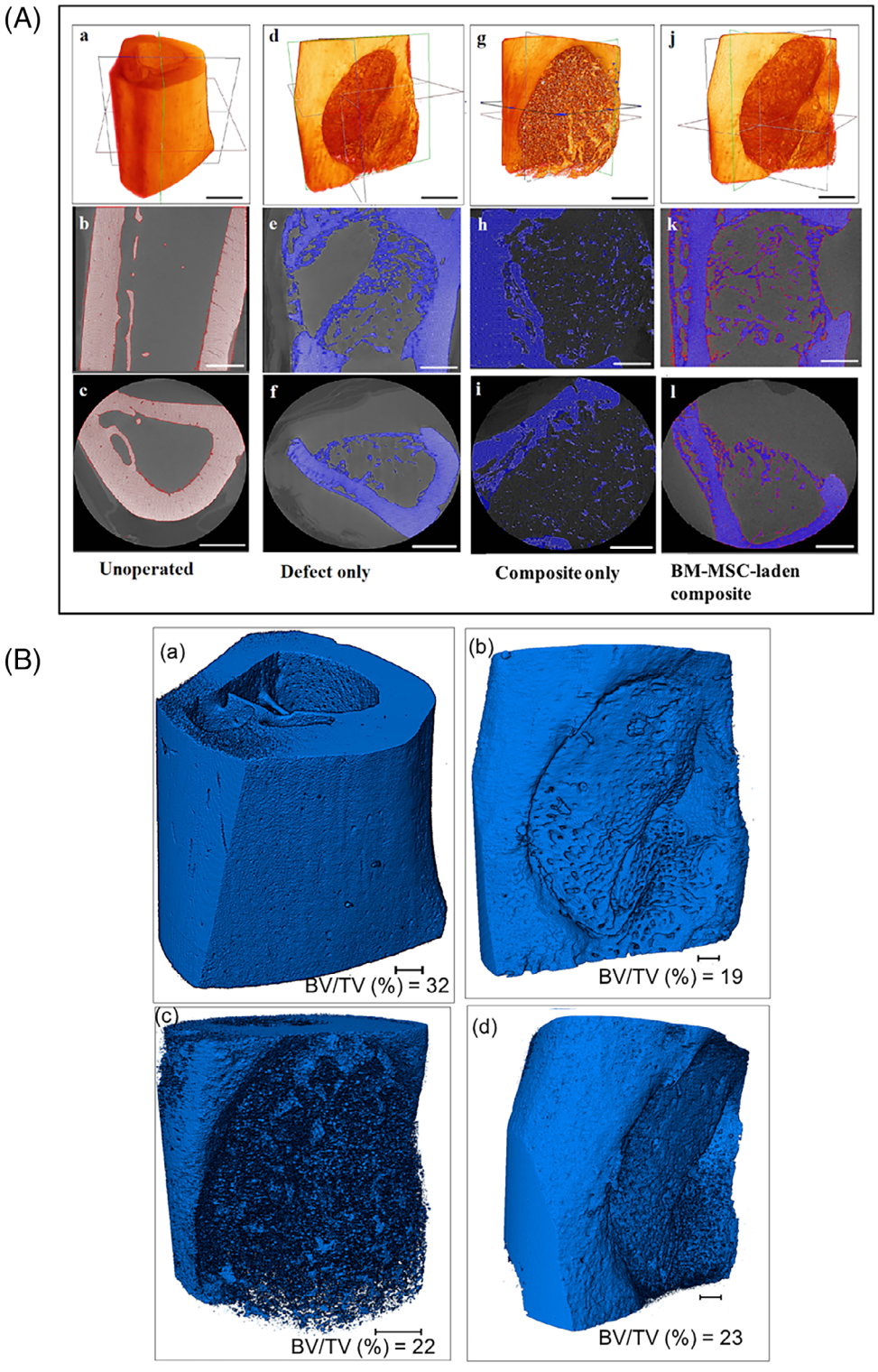

FIGURE 6 A, Microcomputed tomographs showing series of 3D reconstructions of rat tibial bone (a, b,g,j) with locations of sagittal (Y-Z plane) sections (b,e,h,k) and trans-axial (X-Y plane) sections (c,f,i,l) before and after implantation of the composite. The imaging was performed after 6 weeks of BM-MSC-laden CHT/HA/PCL composite implantation. Scale bar is 500 μm. B, Representative images showing 3D reconstruction of rat tibia after various image-processing steps showing three-dimensional morphologies of (a) unoperated bone, (b) defect only, (c) composite only, and (d) composite with undifferentiated BM-MSCs after implantation of 6 weeks. Bone volume to total volume ratio (BV/TV) was calculated after volume rendering and thresholding. Scale bar is 500 μm

3.3.1 | Micro-CT data

The representative images of micro-CT of rat tibiae following 6 weeks of implantation are illustrated in Figure 6. The quantitative analysis of the micro-CT results has been done mentioning bone volume to the total volume ratio (BV/TV), also known as bone volume fraction, which is the most relevant morphologic value in the characterization of trabecular bone (Figure 6B). In Figure 6A, from top to bottom, transects shown in the 3D images denote a longitudinal and a transverse section of the same tibia at 6 weeks of unoperated leg (a-c), defect only (d-f), composite only (g-i), and BM-MSC-laden composite (j-l), respectively. Bone is very much compact with full trabecular thickness in unoperated leg (Figure 6A,a-c). An unoperated tibia was scanned as a positive control that showed a full-thickness cortical bone in the ROI with BV fraction percentage (BV/TV%) of 32 (Figure 6B,a), whereas, sham control was taken as tibia without composite. The micro-CT images indicate the morphological features of intramedullary rat

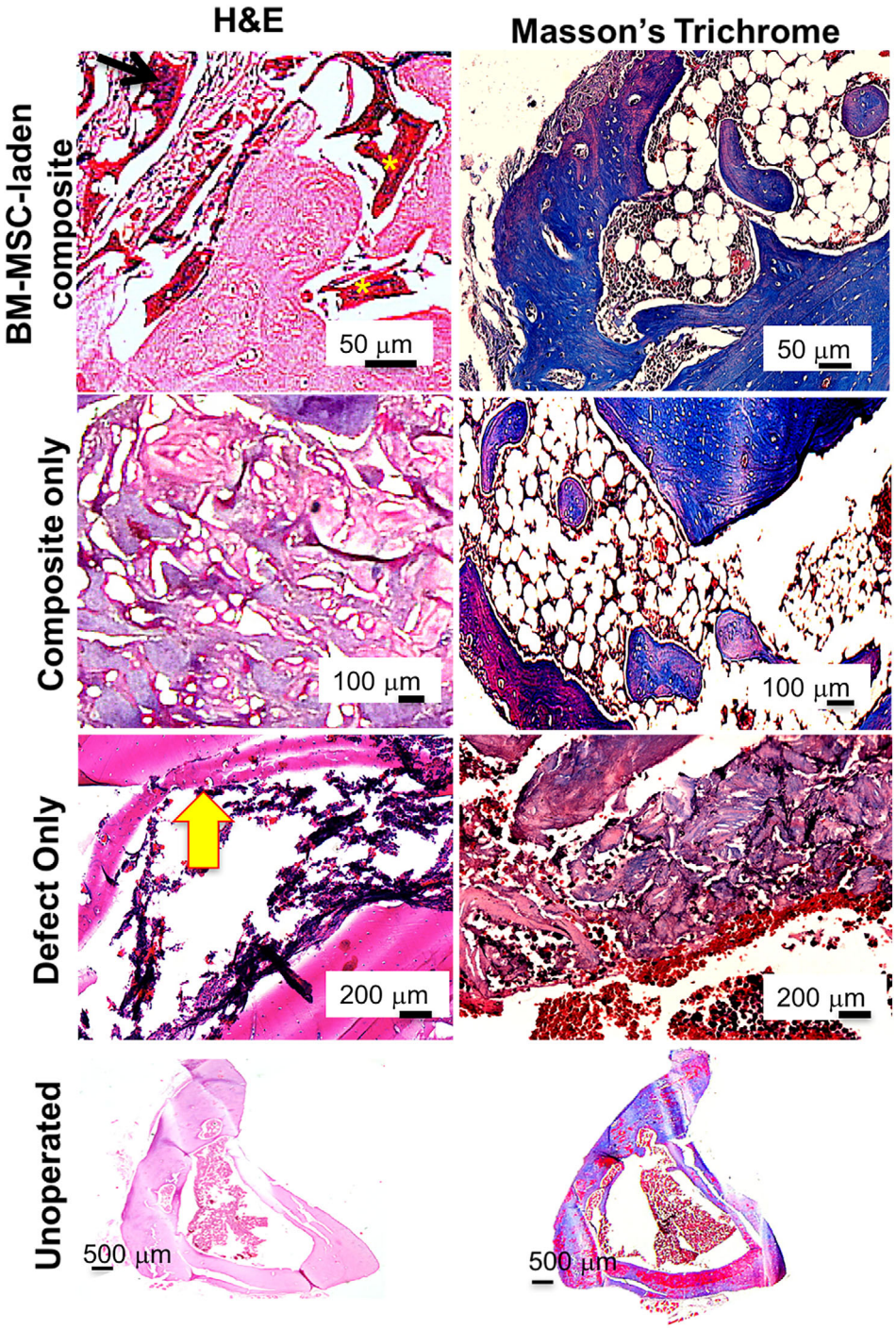

FIGURE 7 Histology micrographs of ex vivo samples of BM-MSC-laden CHT/HA/PCL implanted rat tibiae harvested 6 weeks post surgery. The left side panel depicts H&E staining and Masson's trichrome staining is on the right side panel. CHT, chitosan; HA, hydroxyapatite; H&E, hematoxylin and eosin; PCL, polycaprolactone

tibial control defect which is of a 3 mm size (without implanted biomaterial) with minimal evidence of osseointegration (Figure 6A, d-f). For comparison, the as-synthesized composite without stem cells is also taken in our in vivo study (Figure 6A,g-i). After 6 weeks of healing, the obtained micro-CT images indicated that bone regeneration was marginally greater in quality as well as quantity in both the groups (composite only and BM-MSC laden composite), when compared to control group. But the micro-CT images show greater trabecular construction with more organized supporting bone around the BM-MSC-laden composite (Figure 6A, j-l). Rats implanted with composite only showed 16% increase in the trabecular BV/TV with 0.22 value when compared with that of rats with defect only (BV/TV% of 19) (Figure 6B,b). The ossification occurred in the form of small islands of mineralized tissue formation, which appeared as high contrast particles in the micro-CT data. When the composites were implanted with BM-MSCs, not much difference was observed in terms of total bone formation, based on qualitative examination. However, quantitatively, the BV fraction got elevated by 21%, when compared to defect-only group (Figure 6B). A clear examination of high-resolution 3D images acquired from micro-CT clearly indicated significantly faster bone regeneration at 6 weeks for both composite-only group and BM-MSC-laden composite group.

3.3.2 | Histological evaluation of constructs

Unoperated leg, without defect, served as positive control for histology showing mature tibial bone. The control group, without composite, depicted thin septa of immature bone formation in 6 weeks (yellow arrow). In the composite only group, H&E staining showed small bony islands inside the defect area (Figure 7). Neo-bone formed in close association with the composite, as also indicated by micro-CT (Figure 6). Large fragments of composite remained occupying majority of defect area suggesting controlled degradation up to 6 weeks. Masson's Trichrome staining of the composite only group revealed immature bone formation (Figure 7). When BM-MSC-laden composites were implanted, improved bone formation was evident as compared to the composite-only group. The fragments of the composite (Figure 7; yellow asterisk) were significantly less evident, with more neobone occupying the defect area. The presence of the cells on the surface of the composite was conspicuous in several places (Figure 7; black arrow).

4 | DISCUSSION

Osteogenic regeneration using hMSC progenitors in the form of direct cell injections suffer from major limitations such as heterogeneous cellular differentiation, and leakage into other sites. This has triggered the need for biomaterials to serve as bone substitutes offering biocompatibility with desired mechanical properties mimicking the target tissue. Medical-grade PCL and associated composites (such as HA) have received FDA approval and are extensively used in bone tissue engineering.[47] Therefore, tuning PCL-based materials to improve upon the existing material properties will yield a composite with higher chances of clinical acceptance.[4,16,48] Bioactive composites of PCL have demonstrated osteopromotive properties towards bone formation compared to hydrogels and ceramics.[49,50] Our earlier studies demonstrated that a multimaterial composite of PCL, CHT, and HA facilitated osteogenic differentiation of seeded BM-MSCs in vitro, and ectopic implantation in subcutaneous rat model revealed calcification around the implant.[16,48] However, the composite failed to demonstrate mature differentiation of seeded progenitors toward phenotypically stable osteocytes. These findings intrigued us to design an improved composite with better biocompatibility to guide cell differentiation. This study focuses on a slightly modified ratio of the composite (3:3:2 ratio of CHT/HA/PCL) and tests its potential towards inducing mature osteogenic differentiation in vitro and in an orthotopic load-bearing defect model in vivo. These aspects were not studied before. We further conducted a comparative analysis of the three most promising tissue-specific hMSCs, that is, BM-MSCs, AD-MSCs, and WJ-MSCs for in vitro bone regeneration. Only few studies have reported direct comparison of the osteogenic potential of the three MSC sources on 3D composites.[51] Therefore, we believe that this is the first, concrete evidence dictating superior osteogenesis in BM-MSC-laden composites to fabricate phenotypically stable bone tissue constructs. CHT/HA/PCL composites mitigate the lack of adequate osteoconductivity associated with PCL-only scaffolds, weaker mechanical properties of CHT and brittleness of pure HA, while rendering ease of fabrication and, customizability together with better biocompatibility.

4.1 | In vitro stem cell progenitor-dependent osteogenesis modulation

Unlike BM-MSCs, which generally differentiate more readily into skeletal tissues (bone and cartilage), the osteogenic capacity of AD-MSCs and WJ-MSCs is less evident. Having relatively more convenient and patient-friendly processing parameters, the clinical field will highly benefit if such cell sources become mainstay in orthopedic surgeries. This limitation motivated us to perform studies that seek to evaluate the osteogenic potential of AD-MSCs and WJ-MSCs in 3D scaffolds. Here, we showed that all three MSC types adhered to the composite surface exhibiting increased viability over the 21-day culture period. Marked increase in cell density, followed by a thick layer of Col I in all the three MSC-laden cell constructs was observed, though to variable extents. Maximal ECM was noted in BM-MSC- and AD-MSC-laden composites. Further analysis of the composites by immunostaining confirmed mineralization (OCN, Figure 4B) and EDX showed the ratio of Ca/P as 1:3, lesser than pure HA (Figure 3B). Due to complete cell coverage and the presence of HA particles on the composite surface, it was possible to obtain only overall Ca/P ratio. Moreover, BM-MSCs

seeded on the composite showed phenotypic transition into mature osteocytes, marked by shape modulation (fibroblastic to stellate shaped) (Figure 3A) and positive expression of SOST,[1] marker for mature osteocytes (Figure 4B). In native bone, osteocytes form primarily after the mineralization stage, and get encapsulated within the calcified matrix of cortical bone as terminally differentiated bone cells. These cells play critical role in mechanosensing, ion transportation, and maintaining bone homeostasis.[52] While most studies related to bone tissue engineering demonstrate cytocompatibility and calcification by seeded bone cells, there is limited literature available on the propensity of such composites to drive cells towards terminally differentiated phenotype.[1,20] Relatively inferior bone differentiation in AD-MSCs and WJ-MSCs in vitro was marked by lack of phenotypic transition into mature cells, both morphologically (Figure 3A) and at the molecular level (Figure 4). The combination of the morphology of cells, mineral formation, gene expression profile coupled with positive staining for bone markers and the Ca/P ratio indicate that the matrix produced by the BM-MSC-laden composites had mineralized and the cells were terminally differentiated, in vitro.

It is known that canonical Wnt/β-catenin signaling is imperative in dictating the fate of MSCs.[53] MSCs proliferating in low Wnt/β-catenin conditions trigger increased pluripotency genes (*Oct-4*, *Sox-2*, and *Nanog*),[54,55] whereas high Wnt/β-catenin conditions tend to differentiate cells towards a more committed osteoblast-like stage. WJ-MSCs displayed decreased cellular senescence in vitro (Figure 2), increased cell viability and reduced differentiation (Figures 3,4), as reported before by others.[56] These could be explained, at least partly, by the aberrant expression of β-catenin signaling in WJ-MSCs. Two other genes associated with the canonical Wnt signaling, *AXIN2*, and *porcupine homolog 1*, are significantly downregulated in WJ-MSCs,[56] inhibiting cellular differentiation. On the other hand, β-CATENIN synthesis was more promising in BM-MSCs than AD-MSCs, after 14 days of in vitro culture. Concurrently, BM-MSCs also demonstrated an increase in *BMP-4* mRNA levels. Previous reports have associated this synergistic interaction between β-CATENIN and *BMP-4* expression levels in BM-MSCs seeded on 3D gelatin foams (incorporated with Ca^{2+} ions) to calcium-dependent signaling effect that induces an increased osteogenic outcome.[57] The Ca^{2+} ions in our study originated from the HA component. AD-MSCs and WJ-MSCs, on the contrary, failed to express significant levels of *BMP-4* and β-CATENIN (BM-MSCs > AD-MSCs > WJ-MSCs). These findings are in accordance with previous reports indicating reduced osteogenic differentiation capacity of WJ-MSCs and AD-MSCs in comparison to BM-MSCs.[15,58] While comparisons between cell cycle-related genes of WJ-MSCs with other MSC types (such as BM-MSCs) is done before,[56] their tendency to differentiate into osteogenic lineage on a 3D substrate with appropriate milieu gave further insights into their slower clinical progression towards regenerative therapy. Co-delivery of additional osteogenic moieties may be effective in inducing differentiation of fetal WJ-MSCs, which are of primitive origin as compared to the more specialized BM-MSCs and AD-MSCs. BM-MSCs, so far, provided consistent data for osteogenic differentiation, which have been effectively put to use in clinical therapy.

4.2 | Early osseointegration in rat model

Based on the in vitro screening data, the CHT/HA/PCL scaffolds were evaluated in vivo with and without BM-MSCs where our data demonstrated partial bone healing of rat tibial defects within 6 weeks (Figures 5-7). The added advantage of coupling undifferentiated hMSCs to 3D composites has previously been reported.[59] Kang et al reported significantly higher mRNA levels of *OCN* and *ALP* when undifferentiated MSC-laden poly(lactic-co-glycolic acid)/HA (PLGA/HA) composites were implanted in vivo as compared to differentiated MSC-laden scaffolds.[59] From the clinical perspective, added advantage of using undifferentiated MSC population with bone constructs is reduced culture period resulting in lesser waiting time for patients and avoiding the use of additional chemicals such as dexamethasone, which may administer cytotoxic effects in the patient's body.

The defect model chosen was a subcritical defect, which will automatically repair within 12 weeks.[21] The time point of 6 weeks was primarily chosen to identify the early phase responses of the material-bone integration. There was good material-bone contact and the composites seemed to be strongly integrated within the defect site, as observed at the time of tibial harvestation. This was further corroborated with quantitative micro-CT analysis (Figure 6). The present results are in accordance with the study of Duan et al.[60] who have also reported that the BM-MSC sheets combined with titanium implants showed improved implant osseointegration in an ovariectomized rat model of osteoporosis. In their study, micro-CT indicated that BV/TV (%) of BM-MSC-implant test group (30.7) was significantly higher than implant-only, without BM-MSC incorporation (12.8). This result clearly demonstrated quantitative evidence of greater trabecular construction over a healing period of 8 weeks, when compared with those in the control group (9.76).[60] Similar to this, our results also indicated the efficacy of porous composites for bone regeneration, that is, osteogenesis due to infiltration of BM-MSCs. The BV/TV values for rat tibia for various implant constructs are comparable with those shown by Duan et al.[60]

Furthermore, one important observation is that the extent of bone growth is nonidentical in different animal species even if the implantation site is same. For example, BV/TV observed around the implants in rat tibial defects is lower than those conducted on rabbit model. The rate of bone colonization or bone ingrowth is dependent upon various critical parameters in the implantation sites which includes bone architecture and biomechanical forces with initial bone–implant contact.[61] In one of our earlier in vivo studies in a rabbit model, we have reported a significant increase in the BV/TV ratio from 0.62 to 0.81 and 0.77 to 0.80 in rabbit femur around LG26Sr (glass ceramic) and HA-based bioglass, respectively from 4 to 12 weeks.[62] BV/TV ratio shown in rabbit model is higher than those observed in rats. This clearly shows that the bone ingrowth at the implantation site is not only dependent on the animal model, but also the architecture of the host bone. Furthermore, Guehennec et al.[61] have

reported a comparative study in rats and rabbits (two different animal species), on the bone colonization of a macroporous biphasic calcium phosphate ceramic implanted in different sites such as femur, tibia, and calvaria. Bone growth was observed in all the implantation sites, that is, femur, tibia, and calvaria of rats but the bone colonization has been reported statistically elevated in the femur of rabbits than in the tibial and calvarial areas. Also, the bone growth has been reported higher in rabbits than in rats, which might be attributed due to the large bone surface area in contact with the samples.[61]

4.3 | Scaffold structure and composition-dependent biocompatibility

Another interesting observation was that the cell-laden composites appeared more degraded, compared to composite-only group after 6 weeks of implantation. BM-MSCs, either secrete cytokines that aid in bone formation or directly differentiate into osteoblasts. In addition, they are capable of differentiating into endothelial cells to enhance the functionality of new bone.[63] Zhang et al[64] demonstrated that porous silk-based scaffolds could promote enhanced bone healing in rat cranial defects, only when seeded with cells. Only silk scaffold did not demonstrate bone formation in vivo. On the contrary, PCL-based scaffolds have previously failed to retain cells on the scaffold surface within weeks of implantation, which may be attributed to the inadequate surface chemistry of the scaffold.[65] Whereas, in our study, the amount of bone ingrowth was significantly higher for BM-MSC-laden composites, indicating that the composites were indeed successful in retaining the cells on the surface, which aided in superior bone formation.

Besides cellular cues, physical cues have also attracted significant attention due to their ability to alter cell shape, gene expression through ECM-cell interactions and lineage commitment of the cells. Interactions between the biological fluid and the material surface are often mediated by proteins adsorbed from the fluid. Creating surface topographies with features mimicking the size of proteins enhance the rate of adsorption. A study reported an increased osteoblast adherence up to three-fold on the surface of nanosized titanium particles in comparison to conventional titanium particles.[66] In addition, surface roughness (in the range of nano- to microscale) are critical in promoting osteogenesis.[67] Hence, the presence of HA in the composite is an important determinant of protein and cellular adsorption due to hydrophilicity, rougher surface, and source of Ca and P ions for osteoinduction.[68] Formation of biological carbonated apatite layer, facilitated by HA-fluid interaction triggers stem cells either to directly differentiate along the bone lineage or to trigger the release of biological factors to facilitate the process. Next, adequate porosity (80%-90%) and pore size (>100 μm) are crucial for scaffolds in order to allow sufficient vascularization and fluid exchange throughout the composite, which our composite seems to satisfy.[69] In a slightly different in vitro setup, Ardeshirylajimi et al demonstrated an increased expression of osteogenic markers (*ALP*, *Runx2*, *Osteonectin*, *OCN*) over 21-day culture period in freeze-dried 3D porous CHT-based scaffolds seeded with AD-MSCs with 10% porosity and pore size of 80 ± 20 μm, as opposed to 15% and 20% porosities, respectively. CHT, with lesser rigidity than PCL, may not be able to render comparable mechanosensing required for osteogenic differentiation of cultured cells. This response will further weaken as the porosity is increased. Therefore, the choice of a different base substrate may not allow appropriate comparison between the two studies.[70] The preliminary permeability tests conducted on our composite with varying heights (4 and 8 mm) provided evidence of restricted fluid flow with an increase in height of the composite. This may subsequently result in necrotic core, a problem prevalent in clinic with most critical-sized defects.[71] However, it is noteworthy that in vivo bone microenvironment is dynamic in nature with constant fluid flow. Therefore, future studies should emphasize on the presence of dynamic testing conditions for the scaffolds; akin to in vivo physiological bone model.

5 | CONCLUSIONS

Though several commercial biomaterials (such as PCL) have benefited patients, but even after decades, the production of anatomical-sized constructs for large bone defects remains a challenge. We successfully demonstrated that 3D porous CHT/HA/PCL can serve as a potential bone analog. Clinicians often combine biomaterials with autologous stem cells for fully vascularized bone healing. However, using optimal cell source and modulating the stem cell behavior towards achieving maximal differentiation can significantly alter the extent of osteogenesis under clinical settings. Though our ultimate aim was to provide a comparable clinical alternative to the popular BM-MSCs using lesser invasive tissue sources, BM-MSCs seemed to behold unmatched osteogenic properties marked by terminal bone differentiation, distinct gene expression, and strong bone-material interface for early bone formation. The study warrants further investigation into the material using higher-order animal models for validating their osteogenic potential in critical-sized defects.

ACKNOWLEDGMENTS

Swati Midha was supported by DST (DST/INSPIRE/04/2017/000645), Amtoj Kaur was supported by CSIR (09/006(0478)/2018-EMR-I) and Prof. Sujata Mohanty was supported by DBT (BT/01/COE/07/03). One of the authors Nitu Bhaskar would like to acknowledge the funding received from DST (SR/WOS-A/LS-513/2017) for her research work and also, Gowtham NH for help in micro-CT analysis. The authors would like to acknowledge support from Central Animal Facility and Central Instrumentation Facility (SEM) at AIIMS, New Delhi, Central Instrumentation Facility (Confocal Microscope) at Delhi University South Campus and IGIB Institute, Mathura Road, NRF Facility (XRD) at IIT Delhi. We also acknowledge Mr. Ravindra Meena's assistance in XRD and FTIR data.

CONFLICT OF INTEREST

The authors declared no potential conflicts of interest.

AUTHOR CONTRIBUTIONS

S. Midha: conception and design, financial support, collection and/or assembly of data, data analysis and interpretation, manuscript writing; K.G.J., N.B.: collection and/or assembly of data, data analysis and interpretation related to Micro-CT results only, manuscript writing (specific sections); A.K., S.R.: collection and/or assembly of data, data analysis and interpretation; S.G.: data analysis and interpretation, financial support, manuscript proofreading. B.B.: data interpretation (specific sections related to Micro-CT). S. Mohanty: conception and design, financial support, administrative support, provision of study material or patients, final approval of manuscript.

DATA AVAILABILITY STATEMENT

The data that support the findings of this study are available from the corresponding author upon reasonable request.

ORCID

Swati Midha https://orcid.org/0000-0003-0295-5356
Shibashish Giri https://orcid.org/0000-0003-2107-7595
Sujata Mohanty https://orcid.org/0000-0002-0047-4914

REFERENCES

1. Midha S, Murab S, Ghosh S. Osteogenic signaling on silk-based matrices. *Biomaterials*. 2016;97:133-153.
2. Heydari Z, Mohebbi-Kalhori D, Afarani MS. Engineered electrospun polycaprolactone (PCL)/octacalcium phosphate (OCP) scaffold for bone tissue engineering. *Mater Sci Eng C*. 2017;81:127-132.
3. Haghjooy Javanmard S, Anari J, Zargar Kharazi A, Vatankhah E. *In vitro* hemocompatibility and cytocompatibility of a three-layered vascular scaffold fabricated by sequential electrospinning of PCL, collagen, and PLLA nanofibers. *J Biomater Appl*. 2016;31:438-449.
4. Jin RM, Sultana N, Baba S, et al. Porous PCL/chitosan and nHA/PCL/chitosan scaffolds for tissue engineering applications: fabrication and evaluation. *J Nanomater*. 2015;2015, Article ID 357372:8 pages.
5. S N, M M, Hwan JK, et al. Characterization of 3D printed PLA/PCL/TiO2 composites for Cancellous bone. *J Mater Sci Eng*. 2018;7:417-426.
6. Linh NTB, Min YK, Lee BT. Hybrid hydroxyapatite nanoparticles-loaded PCL/GE blend fibers for bone tissue engineering. *J Biomater Sci Polym Ed*. 2013;24:520-538.
7. Aranaz I, Mengibar M, Harris R, et al. Functional characterization of chitin and chitosan. *Curr Chem Biol*. 2012;3:203-230.
8. Ronca D, Langella F, Chierchia M, et al. Bone tissue engineering: 3D PCL-based nanocomposite scaffolds with tailored properties. *Procedia CIRP*. 2016;49:51-54.
9. Meirelles L, Arvidsson A, Andersson M, Kjellin P, Albrektsson T, Wennerberg A. Nano hydroxyapatite structures influence early bone formation. *J Biomed Mater Res A*. 2008;87:299-307.
10. Strioga M, Viswanathan S, Darinskas A, et al. Same or not the same? Comparison of adipose tissue-derived versus bone marrow-derived mesenchymal stem and stromal cells. *Stem Cells Dev*. 2012;21:2724-2752.
11. Liao HT. Osteogenic potential: comparison between bone marrow and adipose-derived mesenchymal stem cells. *World J Stem Cells*. 2014;6:288-295.
12. Mohamed-Ahmed S, Fristad I, Lie SA, et al. Adipose-derived and bone marrow mesenchymal stem cells: a donor-matched comparison. *Stem Cell Res Ther*. 2018;9:168.
13. Ansari AS, Yazid MD, Sainik NQAV, Razali RA, Saim AB, Idrus RBH. Osteogenic induction of Wharton's jelly-derived mesenchymal stem cell for bone regeneration: a systematic review. *Stem Cells Int*. 2018;2018:1-17.
14. Xie X, Wang Y, Zhao C, et al. Comparative evaluation of MSCs from bone marrow and adipose tissue seeded in PRP-derived scaffold for cartilage regeneration. *Biomaterials*. 2012;33:7008-7018.
15. Kern S, Eichler H, Stoeve J, et al. Comparative analysis of Mesenchymal stem cells from bone marrow, umbilical cord blood, or adipose tissue. *Stem Cells*. 2006;24:1294-1301.
16. Jain KG, Mohanty S, Ray AR, Malhotra R, Airan B. Culture and differentiation of mesenchymal stem cell into osteoblast on degradable biomedical composite scaffold: *in vitro* study. *Indian J Med Res*. 2015;142:747-758.
17. Sahu N, Baligar P, Midha S, et al. Nonmulberry silk fibroin scaffold shows superior osteoconductivity than mulberry silk fibroin in calvarial bone regeneration. *Adv Healthc Mater*. 2015;4:1709-1721.
18. Paliwal S, Chaudhuri R, Agrawal A, Mohanty S. Human tissue-specific MSCs demonstrate differential mitochondria transfer abilities that may determine their regenerative abilities. *Stem Cell Res Ther*. 2018;9:298-308.
19. Midha S, Chawla S, Chakraborty J, et al. Differential regulation of hedgehog and parathyroid signaling in mulberry and non-mulberry silk fibroin textile braids. 2018;4:595-607.
20. Midha S, Chameettachal S, Dey E, Ghosh S. Nonmulberry silk braids direct terminal Osteocytic differentiation through activation of Wnt-signaling. *ACS Biomater Sci Eng*. 2017;3:1062-1074.
21. Midha S, Kim TB, Van Den Bergh W, et al. Preconditioned 70S30C bioactive glass foams promote osteogenesis in vivo. *Acta Biomater*. 2013;9:9169-9182.
22. Midha S, Tripathi R, Geng H, Lee PD, Ghosh S. Elucidation of differential mineralisation on native and regenerated silk matrices. *Mater Sci Eng C*. 2016;68:663-674.
23. Catledge SA, Clem WC, Shrikishen N, et al. An electrospun triphasic nanofibrous scaffold for bone tissue engineering. *Biomed Mater*. 2007;2:142-150.
24. Xia Y, Zhou PY, Cheng XS, et al. Selective laser sintering fabrication of nano-hydroxyapatite/poly-ε-caprolactone scaffolds for bone tissue engineering applications. *Int J Nanomed*. 2013;8:4197–4213.
25. Patel S, Jammalamadaka U, Sun L, et al. Sustained release of antibacterial agents from doped halloysite nanotubes. *Bioengineering*. 2015,3:pii: E1.
26. Drouet C. Apatite formation: why it may not work as planned, and how to conclusively identify apatite compounds. *Biomed Res Int*. 2013;2013:1-12.
27. Shahabi S, Najafi F, Majdabadi A, et al. Effect of gamma irradiation on structural and biological properties of a PLGA-PEG-hydroxyapatite composite. *Sci World J*. 2014;2014:1-9.
28. Fraga AF, Filho EDA, Rigo ECDS, et al. Synthesis of chitosan/hydroxyapatite membranes coated with hydroxycarbonate apatite for guided tissue regeneration purposes. *Appl Surf Sci*. 2011;257:3888-3892.
29. Aliah NN, Ansari MNM. Thermal analysis on characterization of polycaprolactone (PCL)—chitosan scaffold for tissue engineering. *Int J Sci Res Eng Technol*. 2017;6:76-80.
30. Wu Y, Sriram G, Fawzy AS, et al. Fabrication and evaluation of electrohydrodynamic jet 3D printed polycaprolactone/chitosan cell carriers using human embryonic stem cell-derived fibroblasts. *J Biomater Appl*. 2016;31:181-192.

31. Kumar S, Koh J. Physiochemical, optical and biological activity of chitosan-chromone derivative for biomedical applications. *Int J Mol Sci*. 2012;13:6102-6116.
32. Nazeer MA, Yilgör E, Yilgör I. Intercalated chitosan/hydroxyapatite nanocomposites: promising materials for bone tissue engineering applications. *Carbohydr Polym*. 2017;175:38-46.
33. Maji K, Dasgupta S, Kundu B, Bissoyi A. Development of gelatin-chitosan-hydroxyapatite based bioactive bone scaffold with controlled pore size and mechanical strength. *J Biomater Sci Polym Ed*. 2015;26:1190-1209.
34. Sarasam AR, Krishnaswamy RK, Madihally SV. Blending chitosan with polycaprolactone: effects on physicochemical and antibacterial properties. *Biomacromolecules*. 2006;7:1131-1138.
35. Paladino FV, Sardinha LR, Piccinato CA, et al. Intrinsic variability present in Wharton's jelly mesenchymal stem cells and T cell responses may impact cell therapy. *Stem Cells Int*. 2017, 2017, Article ID 8492797:12 pages.
36. Wang Q, Yang Q, Wang Z, et al. Comparative analysis of human mesenchymal stem cells from fetal-bone marrow, adipose tissue, and Warton's jelly as sources of cell immunomodulatory therapy. *Hum Vaccines Immunother*. 2016;12:85-96.
37. Qu C, Kaitainen S, Kröger H, Lappalainen R, Lammi M. Behavior of human bone marrow-derived mesenchymal stem cells on various titanium-based coatings. *Materials*. 2016;9:pii: E827.
38. Schaffler MB, Cheung WY, Majeska R, et al. Osteocytes: master orchestrators of bone. *Calcif Tissue Int*. 2014;94:5-24.
39. Golub EE, Boesze-Battaglia K. The role of alkaline phosphatase in mineralization. *Curr Opin Orthop*. 2007;18:444–448.
40. Boukhechba F, Balaguer T, Michiels JF, et al. Human primary osteocyte differentiation in a 3D culture system. *J Bone Miner Res*. 2009;24:1927-1935.
41. Szöke K, Daňková J, Buzgo M, Amler E, Brinchmann JE, Østrup E. The effect of medium composition on deposition of collagen type 1 and expression of osteogenic genes in mesenchymal stem cells derived from human adipose tissue and bone marrow. *Process Biochem*. 2017;59:321-328.
42. Lee JW, Chu SG, Kim HT, et al. Osteogenesis of adipose-derived and bone marrow stem cells with polycaprolactone/tricalcium phosphate and three-dimensional printing technology in a dog model of maxillary bone defects. *Polymers*. 2017;9:450-466.
43. Zhou Y, Guan X, Zhu Z, et al. Osteogenic differentiation of bone marrow-derived mesenchymal stromal cells on bone-derived scaffolds: effect of microvibration and role of ERK1/2 activation. *Eur Cells Mater*. 2011;22:12-25.
44. Farhadieh RD, Gianoutsos MP, Yu Y, Walsh WR. The role of bone morphogenetic proteins BMP-2 and BMP-4 and their related post-receptor signaling system (Smads) in distraction osteogenesis of the mandible. *J Craniofac Surg*. 2004;15:714-718.
45. Szepesi Á, Matula Z, Szigeti A, et al. *In vitro* characterization of human mesenchymal stem cells isolated from different tissues with a potential to promote complex bone regeneration. *Stem Cells Int*. 2016, 2016, Article ID 3595941, 9 pages.
46. Wang Q, Zhao G, Xing Z, et al. Comparative evaluation of the osteogenic capacity of human mesenchymal stem cells from bone marrow and umbilical cord tissue. *Exp Ther Med*. 2018;17:764-772.
47. Henkel J, Woodruff MA, Epari DR, et al. Bone regeneration based on tissue engineering conceptions—a 21st century perspective. *Bone Res*. 2013;1:216-248.
48. Jain KG, Singh M, Kakkar A, et al. Evaluating the osteogenic potential of CHT/PCL/HAP biocomposites in bone tissue engineering: an *in vivo* study. *Int J Sci Res*. 2017;6:10-13.
49. Liu M, Zeng X, Ma C, et al. Injectable hydrogels for cartilage and bone tissue engineering. *Bone Res*. 2017;5:17014.
50. Prasadh S, Wong RCW. Unraveling the mechanical strength of biomaterials used as a bone scaffold in oral and maxillofacial defects. *Oral Sci Int*. 2018;15:48-55.
51. Ardeshirylajimi A, Mossahebi-Mohammadi M, Vakilian S, et al. Comparison of osteogenic differentiation potential of human adult stem cells loaded on bioceramic-coated electrospun poly (L-lactide) nanofibres. *Cell Prolif*. 2015;48:47-58.
52. Florencio-Silva R, Sasso GRDS, Sasso-Cerri E, et al. Biology of bone tissue: structure, function, and factors that influence bone cells. *Biomed Res Int*. 2015;2015:1-17.
53. Zhou S. TGF-β regulates β-catenin signaling and osteoblast differentiation in human mesenchymal stem cells. *J Cell Biochem*. 2011;112:1651-1660.
54. Greco SJ, Liu K, Rameshwar P. Functional similarities among genes regulated by Oct4 in human mesenchymal and embryonic stem cells. *Stem Cells*. 2007;25:3143-3154.
55. Tsai CC, Su PF, Huang YF, Yew TL, Hung SC. Oct4 and nanog directly regulate Dnmt1 to maintain self-renewal and undifferentiated state in mesenchymal stem cells. *Mol Cell*. 2012;47:169-182.
56. Batsali AK, Pontikoglou C, Koutroulakis D, et al. Differential expression of cell cycle and WNT pathway-related genes accounts for differences in the growth and differentiation potential of Wharton's jelly and bone marrow-derived mesenchymal stem cells. *Stem Cell Res Ther*. 2017;8:102-119.
57. Aquino-Martínez R, Artigas N, Gámez B, Rosa JL, Ventura F. Extracellular calcium promotes bone formation from bone marrow mesenchymal stem cells by amplifying the effects of BMP-2 on SMAD signalling. *PLoS One*. 2017;12:e0178158.
58. Hsieh JY, Fu YS, Chang SJ, et al. Functional module analysis reveals differential osteogenic and stemness potentials in human mesenchymal stem cells from bone marrow and Wharton's jelly of umbilical cord. *Stem Cells Dev*. 2010,19:1895-1910.
59. Kang JM, Kang SW, La WG, et al. Enhancement of *in vivo* bone regeneration efficacy of osteogenically undifferentiated human cord blood mesenchymal stem cells. *J Biomed Mater Res A*. 2010;93:666-672.
60. Duan Y, Ma W, Li D, et al. Enhanced osseointegration of titanium implants in a rat model of osteoporosis using multilayer bone mesenchymal stem cell sheets. *Exp Ther Med*. 2017;14:5717-5726.
61. Le Guehennec L, Goyenvalle E, Aguado E, et al. Small-animal models for testing macroporous ceramic bone substitutes. *J Biomed Mater Res B Appl Biomater*. 2005;72:69-78.
62. Sabareeswaran A, Basu B, Shenoy SJ, et al. Early osseointegration of a strontium containing glass ceramic inarabbit model. *Biomaterials*. 2013;34:9278-9286.
63. Zou D, Zhang Z, He J, et al. Blood vessel formation in the tissue-engineered bone with the constitutively active form of HIF-1α mediated BMSCs. *Biomaterials*. 2012;33:2097-2108.
64. Zhang W, Zhu C, Ye D, et al. Porous silk scaffolds for delivery of growth factors and stem cells to enhance bone regeneration. *PLoS One*. 2014;9:e102371.
65. Dupont KM, Sharma K, Stevens HY, et al. Human stem cell delivery for treatment of large segmental bone defects. *Proc Natl Acad Sci USA*. 2010;107:3305-3310.
66. Puckett S, Pareta R, Webster TJ. Nano rough micron patterned titanium for directing osteoblast morphology and adhesion. *Int J Nanomed*. 2008;3:229-241.
67. Vlacic-Zischke J, Hamlet SM, Friis T, et al. The influence of surface microroughness and hydrophilicity of titanium on the up-regulation of TGFβ/BMP signalling in osteoblasts. *Biomaterials*. 2011;32:665-671.
68. Le Huec JC, Clément D, Brouillaud B, et al. Evolution of the local calcium content around irradiated β-tricalcium phosphate ceramic

implants: *in vivo* study in the rabbit. *Biomaterials*. 1998;19:733-738.
69. Karageorgiou V, Kaplan D. Porosity of 3D biomaterial scaffolds and osteogenesis. *Biomaterials*. 2005;26:5474-5491.
70. Ardeshirylajimi A, Delgoshaie M, Mirzaei S, Khojasteh A. Different porosities of chitosan can influence the osteogenic differentiation potential of stem cells. *J Cell Biochem*. 2018;119:625-633.
71. Kaempfen A, Todorov A, Güven S, et al. Engraftment of prevascularized, tissue engineered constructs in a novel rabbit segmental bone defect model. *Int J Mol Sci*. 2015;16:12616-12630.

SUPPORTING INFORMATION

Additional supporting information may be found online in the Supporting Information section at the end of this article.

How to cite this article: Midha S, Jain KG, Bhaskar N, et al. Tissue-specific mesenchymal stem cell-dependent osteogenesis in highly porous chitosan-based bone analogs. *STEM CELLS Transl Med*. 2021;10:303–319. https://doi.org/10.1002/sctm.19-0385